Sympathetic electromagnetically induced transparency ground state cooling of a $^{40}Ca^{+}$–$^{27}Al^{+}$ pair in an $^{27}Al^{+}$ clock

Chenglong Sun(孙成龙)[1,2,3], Kaifeng Cui(崔凯枫)[1,2,†], Sijia Chao(晁思嘉)[1,2], Yuanfei Wei(魏远飞)[1,2,3], Jinbo Yuan(袁金波)[1,2], Jian Cao(曹健)[1,2], Hualin Shu(舒华林)[1,2], and Xueren Huang(黄学人)[1,2,4,‡]

[1] *State Key Laboratory of Magnetic Resonance and Atomic and Molecular Physics, Innovation Academy for Precision Measurement Science and Technology, Chinese Academy of Sciences, Wuhan* 430071, *China*

[2] *Key Laboratory of Atom Frequency Standards, Innovation Academy for Precision Measurement Science and Technology, Chinese Academy of Sciences, Wuhan* 430071, *China*

[3] *University of Chinese Academy of Sciences, Beijing* 100049, *China*

[4] *Wuhan Institute of Quantum Technology, Wuhan* 430206, *China*

(Received 22 September 2022; revised manuscript received 9 November 2022; accepted manuscript online 17 November 2022)

We report on electromagnetically induced transparency cooling of $^{40}Ca^{+}$ to sympathetically cool the three-dimensional secular modes of motion in a $^{40}Ca^{+}$–$^{27}Al^{+}$ two-ion pair near the ground state. We observe simultaneous ground state cooling across all radial modes and axial modes of a $^{40}Ca^{+}$–$^{27}Al^{+}$ ion pair, occupying a broader cooling range in frequency space over 3 MHz. The cooling time is observed to be less than 1 ms. The mean phonon number and heating rates of all motional modes are measured. This study is not only an important step for reducing the secular motion time-dilation shift uncertainty and uptime ratio of $^{27}Al^{+}$ optical clock, but also essential for high-fidelity quantum simulations and quantum information processors using trapped ions.

Keywords: sympathetic electromagnetically induced transparency cooling, trapped ions, motional ground state; $^{27}Al^{+}$ optical clock

PACS: 06.30.Ft, 37.10.Ty, 37.10.–x **DOI:** 10.1088/1674-1056/aca39d

1. Introduction

Laser-cooled trapped ions are essentially useful in many research fields such as quantum metrology, quantum computation, and quantum simulations.[1–5] In a radio-frequency (rf) driving Paul trap, ions suffer from two kinds of motion:[6] the micromotion driven by the rf field and the secular motion established by the Coulomb interaction between the ions and the trap potential. Shared by all the ions co-trapped in the same trap, the secular motional modes are widely used in transferring information[7] and creating entanglements between ions.[8] Ideally, cooling the ions to the ground state of the secular motion will improve the fidelity of the entanglements[9] and reduce the uncertainty arising from the time-dilation effect,[10] which is nowadays one of the most critical issues in many most advanced trapped ion optical clocks.[11–13]

Various means have been proposed and demonstrated to prepare ions to the motional ground state. To reduce the secular motion time-dilation shift and uncertainty of the $^{27}Al^{+}$ optical clock, the three-dimensional (3D) ground state of the $^{25}Mg^{+}$–$^{27}Al^{+}$ two-ion pair has been achieved.[1] Although traditional sideband cooling[14] and Raman sideband cooling[15] are capable of preparing an ion in a quantum mechanical ground state, those methods typically cool one mode at a time due to their narrow cooling band.[10] In the meantime, other motion modes suffer from heating from the electronic noise[18] and the spontaneous emission,[22] which not only increases the uncertainty of the clock shift but also requires a much longer cooling time.[10]

Another widely used technique for preparing the ions to the motional ground state is electromagnetically induced transparency (EIT) cooling. EIT cooling was first demonstrated theoretically and experimentally for single trapped ions.[19–21] Recently, it has been applied to cool long ion crystal consisting of $^{40}Ca^{+}$ ions[22] and $^{171}Yb^{+}$ ions.[9] It has also been demonstrated to cool neutral atoms in a cavity-QED setup and to cool the oscillators of micro-mechanics.[23] Unlike sideband cooling which requires narrow transitions, EIT cooling allows a wider range of oscillation frequencies for the cooled ion motion. Therefore, multiple motion modes of ion crystals can be simultaneously cooled to low energies, and high cooling rates can be achieved.[16,22] Compared to sideband cooling involving an additional repumping laser, only two lasers are required for EIT cooling, and the required laser power is low.[19]

Here, we demonstrate sympathetically EIT cooling of a pair of $^{40}Ca^{+}$–$^{27}Al^{+}$. Compared with the traditional $^{27}Al^{+}$ ion optical clock scheme based on a $^{25}Mg^{+}$–$^{27}Al^{+}$ ion pair[24,25] and $^{9}Be^{+}$–$^{27}Al^{+}$ ion pair,[17] the lasers involved in the $^{40}Ca^{+}$ experiments are simpler because all lasers of $^{40}Ca^{+}$ required for cooling and detection are easily acquired from external

†Corresponding author. E-mail: cuikaifeng@apm.ac.cn
‡Corresponding author. E-mail: hxueren@apm.ac.cn

© 2023 Chinese Physical Society and IOP Publishing Ltd

cavity diode lasers.[27] The dynamic of cooling long ion chain consisting of $^{40}Ca^+$ has been well investigated,[22] offering a possibility of evaluating the time-dilation shift of the $^{27}Al^+$ with high accuracy.

In this work, all motional modes of a $^{40}Ca^+$–$^{27}Al^+$ ion pair are cooled to the motional ground state. The cooling parameters are optimized to reach the lowest mean quantum number. Cooling times have been observed to be less than 1 ms. We also measured the heating rate of all six modes of a pair of $^{40}Ca^+$–$^{27}Al^+$. Such efficient cooling is essential to reduce the secular motion time-dilation shift of ion optical clocks, such as $^{40}Ca^+$, $^{27}Al^+$, and $^{171}Yb^+$, and is also important for quantum simulation and quantum computing based on trapped ion crystals.

2. Experimental setup

We use a wafer trap that is similar to the one used in NIST's $^{25}Mg^+$–$^{27}Al^+$ clock[24] to form a pair aligned along the trap (z) axis. The distance from the endcap electrode to the ion is 10 mm, and the distance from the radio-frequency (rf) electrode to the ion is 250 μm. The two endcap electrodes are hollow, allowing the laser beam to pass along the trap (z) axis of the ion trap. An aluminum wire and a calcium wire are placed side by side behind one of the endcap electrodes for the ablation loading of both ions with 1064 nm laser. A single $^{40}Ca^+$ ion can be generated directly from the ablation process[29] while a single $^{27}Al^+$ ion needed to be ionized in a two-photon process[3] followed by the ablation pulse.

Our trap is driven by a radio-frequency (rf) frequency of 43.1 MHz. With a loaded Q factor of 220 and 4 W of power fed to the helical resonator, the motional mode frequency of a single $^{40}Ca^+$ is measured to be (2.8, 3.0, 1.0) MHz for the (x, y, z) directions. When trapping a pair of $^{40}Ca^+$ and $^{27}Al^+$, there are two motional modes along each axis: the "common" (COM) mode where mode vectors of the two ions are in the same direction, and the "stretch" (STR) mode where mode vectors of the two ions are opposed. The axial mode frequencies are measured to be 1.17 MHz (COM) and 2.1 MHz (STR), and the radial mode frequencies are in the range of 2.5–4 MHz.[31]

For a $^{40}Ca^+$, a good approximation to such a three-level system is achieved by using the Zeeman sublevels of the $S_{1/2}$ and $P_{1/2}$ manifolds as depicted in Fig. 1(a). The natural linewidth of the $S_{1/2}$ to $P_{1/2}$ transition is $\Gamma = 2\pi \times$ 21.57 MHz.[32] The dressed states are created by a stronger blue-detuned σ^+ polarized light (the dressing laser) coupling the $|P_{1/2}, m = 1/2\rangle$. A π polarized light (the probe laser) coupling the $|S_{1/2}, m = +1/2\rangle$ ground state to the excited state $|P_{1/2}, m = -1/2\rangle$, creates a Fano-type absorption profile. The frequency difference between the EIT dressing light and the probe light is set to match the Zeeman splitting of the ground state in the quantization B-field of 3.6 G. The heating caused by π-polarized light coupling the ground state $|S_{1/2}, m = -1/2\rangle$ and the excited state $|P_{1/2}, m = -1/2\rangle$ can be eliminated as much as possible because the σ^+-polarized light pumps the state from $|S_{1/2}, m = -1/2\rangle$ to $|S_{1/2}, m = +1/2\rangle$. To reduce heating due to the σ-polarized light, the π-polarized light is as perpendicular to the magnetic field as possible.[21]

The levels and transitions in $^{40}Ca^+$ used in the experiment are shown in Fig. 1(b). A laser operating at 397 nm couples the $S_{1/2}$ to $P_{1/2}$ state for Doppler cooling. Repumping from the $D_{3/2}$ state back to the $P_{1/2}$ state is performed by an 866 nm laser beam. The analysis of the motional mode is carried out by exciting the red and blue sideband of the narrow linewidth quadrupole transition from the $S_{1/2}$ state to the $D_{5/2}$ state using a narrow linewidth 729 nm laser referenced to an ultra-stable cavity with Pound–Drever–Hall method. Laser light at 854 nm is used to quench the $D_{5/2}$ state to the short-lived $P_{3/2}$ state. The electronic state readout of the ion uses the well-known electron shelving scheme[33,34] with a photomultiplier tube (PMT).

The top view schematic of the laser beam alignment with respect to the magnetic field is shown in Fig. 1(c). The σ^+-polarized light at 397 nm is oriented parallel to the magnetic field axis. The two laser beams of π-polarized are designed to be perpendicular to the magnetic field axis; which one of the motional modes is cooled depends on the direction of the k vector $(\boldsymbol{k}_\pi - \boldsymbol{k}_\sigma)$. The first π polarized light (397 π1) was designed to cool the axial secular motional modes while the second π polarized light (397 π2) was used to cool the radial modes. Therefore, this experimental setup was designed to allow the cooling of all motional modes.

The 397 nm laser is divided into two laser paths. The σ^+ polarized light lays in the first path where a double-passed acousto-optical modulator (AOM 1) driven at +240 MHz shifts its frequency firstly. Then another single-passed AOM (AOM 2) driven at +110 MHz servers as a shutter and send it to the trap through a fiber. The zero-order diffracted beam of AOM 1 is also shuttered by another double passed AOM (AOM 3) driven at +200 MHz to serve as a far-detuned beam. This can help the ions recrystallize after collision with the background gas.[31] In the second optical path, the 397-nm beam is shifted and shuttered by approximately +260 MHz using another double passed AOM (AOM 4) as the first π polarized light. The zero-order diffracted beam of AOM 4 passes through AOM 5 driven at +260 MHz in a double pass as the second π polarized light. The accurate frequency shift of this AOM is determined by the Zeeman splitting of the $S_{1/2}$ $(m_S = +/-1/2)$ state, which will be calibrated during the experiments. All AOMs are controlled via a field programmable gate array (FPGA) to meet the frequency shifting and power control required for the experiment.

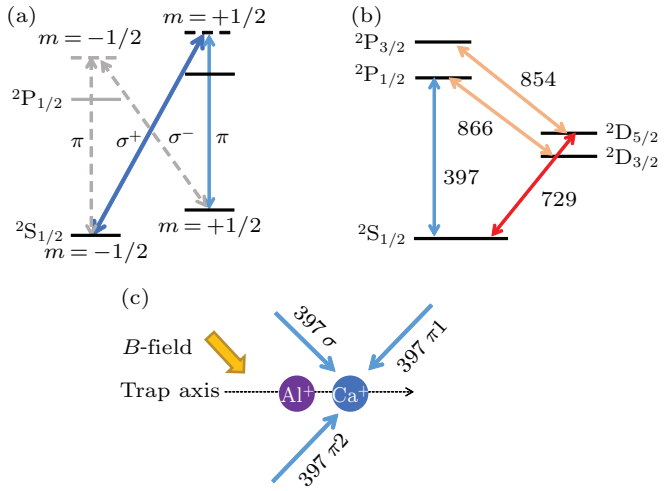


Fig. 1. (a) In $^{40}Ca^+$, the Zeeman sublevels of the $S_{1/2} \rightarrow P_{1/2}$ transition are involved in performing EIT cooling experiments. The σ^+ polarized light is used to create dressed state of the $|S_{1/2}, m = 1/2\rangle$ state, and the $|P_{1/2}, m = +1/2\rangle$ state while π polarized light is used to create the Fano-type absorption profile. (b) Levels and transitions used for the manipulation of $^{40}Ca^+$. A laser at 397 nm in combination with a laser at 866 nm was used for Doppler cooling and detection of the ion. A laser at 854 nm was used for quenching. The motional state analysis is served by a laser at 729 nm. (c) The top view schematic of the laser beam configuration for EIT cooling.

3. Method and results

3.1. EIT cooling principle

EIT cooling requires a three-energy-level structure consisting of two ground states $|S_{1/2}, m = +1/2\rangle$, and $|S_{1/2}, m = +1/2\rangle$, and excited state $|P_{1/2}, m = +1/2\rangle$. The transition $|S_{1/2}, m = +1/2\rangle$ to $|P_{1/2}, m = +1/2\rangle$ is excited by a stronger σ^+ polarization light (dressing laser) at detuning Δ_σ above resonance. The driving field creates dressed state. Then the absorption spectrum on the transition $|S_{1/2}, m = +1/2\rangle$ to $|P_{1/2}, m = +1/2\rangle$ seen by a π polarization light (probe laser) is described by a Fano-type absorption profile.[36] When $\Delta_\sigma = \Delta_\pi$, a dressed state is created and the ac Stark shift created by the dressing laser is[21]

$$\delta = \frac{1}{2}\left(\sqrt{\Delta_\sigma^2 + \Omega_\sigma^2} - |\Delta_\sigma|\right), \tag{1}$$

where Δ_σ is the detuning of the σ^+ polarization light, and Ω_σ is the Rabi frequency. The ac Stark shift δ is made equal to the motional mode frequency ω to be cooled. The EIT cooling dynamics is described by a differential equation for the mean phonon number[37]

$$\dot{\bar{n}} = -\eta^2 (A_- - A_+)\bar{n} + \eta^2 A_+, \tag{2}$$

where $\eta = |\boldsymbol{k}_\pi - \boldsymbol{k}_\sigma| a_0$ is the Lamb–Dicke factor, with a_0 being the rms size of the ground state of the harmonic oscillattor and $\boldsymbol{k}_\sigma$ ($\boldsymbol{k}_\pi$) the dressing (probe) laser wave vector. The coefficients $A_\pm$ are given by[19]

$$A_\pm = \frac{\Omega_\pi^2}{\Gamma} \frac{\Gamma^2\omega^2}{\Gamma^2\omega^2 + 4\left(\frac{\Omega_\sigma^2}{4} - \omega(\omega \mp \Delta)\right)^2}, \tag{3}$$

where Γ is the linewidth of the transition. The steady-state solution of Eq. (2) is $\langle n \rangle = \frac{A_+}{A_- - A_+}$ and the cooling rate is $R = \eta^2 (A_- - A_+)$.[19]

3.2. EIT parameter optimization

To achieve the best EIT cooling performance, the frequency, polarization, and power of all the relevant laser beams must be optimized. Frequency optimization is introduced first. The laser at 397 nm is stabilized in a low-finesse reference cavity with mirror-bonded piezoelectric ceramics (PZT). We scan the driven voltage of this PZT to get the spectral line profile of the $S_{1/2} \rightarrow P_{1/2}$ Doppler cooling transition and park the voltage at resonance. The frequencies of the EIT cooling beam are set equally blue detuned by 75 MHz from the $S_{1/2} \rightarrow P_{1/2}$ resonance.[21] The frequency difference of the EIT cooling beams has to be taken into account due to the Zeeman sublevels splitting. In our experiments, a magnetic field of 3.6 G is used to generate a level splitting of 10 MHz between the $S_{1/2}$ ground state Zeeman levels. The frequency shifting of EIT cooling beams is achieved by acousto-optical modulators as described before.

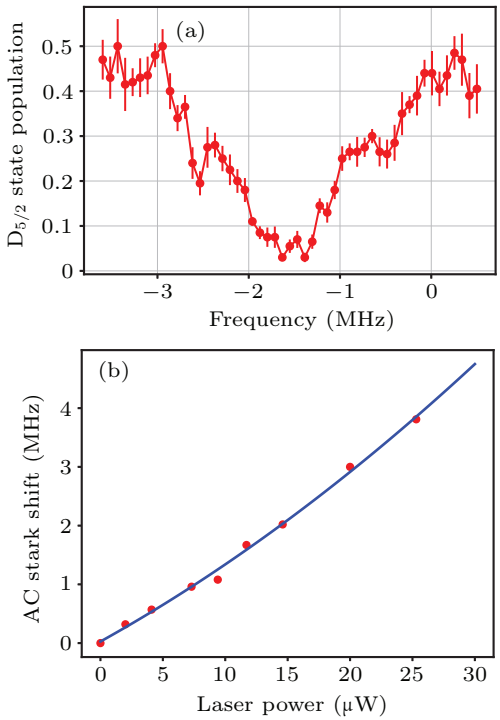


Fig. 2. (a) Measurement of the ac Stark shift induced by the σ^+ polarized light, (b) ac Stark frequency shift as a function of σ^+ polarized light power.

The polarization of both 397 nm laser beams relays on the direction of the quantization axis, which is determined by the direction of the magnetic field. The σ^+ polarized light is set to be circularly polarized using a quarter wave plate and a half wave plate before entering the trap. It has to be aligned with the magnetic field axis. Furthermore, the optimization of the σ^+ polarization light was performed by minimizing

the population of the ion remains on the $|S_{1/2}, m = -1/2\rangle$ state, which is detected by exciting a 729 nm π pulse on the $|S_{1/2}, m = -1/2\rangle \rightarrow |D_{5/2}, m = -5/2\rangle$ transition.

The power of the σ^+ polarized light determines the induced ac Stark shift. Optimal EIT cooling occurs when the ac Stark shift induced by the σ^+ polarized light is equal to the frequency of the vibrational mode. In our experiments, we use a direct way to measure the optical frequency shift by spectroscopy on the ground state $S_{1/2}$ to a metastable state $D_{5/2}$. We drive the transition of $|S_{1/2}, m = -1/2\rangle \rightarrow |D_{5/2}, m = -5/2\rangle$ and switch on the 397 σ^+ polarization beam simultaneously to observe the frequency shift of the $|S_{1/2}, m = -1/2\rangle \rightarrow |D_{5/2}, m = -5/2\rangle$ transition. Figure 2(a) shows the results of one measurement, the 397 σ^+ polarization beam induces an ac Stark shift of 1.5 MHz. The EIT cooling results are largely independent of the intensity of the π polarized light as long as it is much smaller than the σ^+ polarized light intensity.[23] In our experiment, the intensity ratio was $I_\sigma / I_\pi \cong 100$.

3.3. Experimental results

The basic experiment process for EIT cooling consists of five steps.

(i) The ion is Doppler-cooled with the $S_{1/2}$ to $P_{1/2}$ transition. The first π polarized light is set at approximately -10 MHz detuned with respect to the $S_{1/2}$ to $P_{1/2}$ resonant transition. Its intensity is also optimized to reach the lowest Doppler cooling temperature. Doppler cooling was applied for 2 ms.

(ii) To prepare the ion to the $|S_{1/2}, m = 1/2\rangle$ state, optical pumping of 6 μs using the 397 σ^+ beam is applied. The cycle is closed using an 866 nm light.

(iii) The EIT beams of σ^+ polarized light and the first π polarized light and the second π polarized light are applied for EIT cooling.

(iv) State preparation is maintained by using the σ^+ polarized light for an additional 50 μs. Note that the repumping beam at 866 nm is applied to avoid shelving into the $D_{3/2}$ state during steps (i)–(iv).

(v) The quadrupole light at 729 nm is used to analyze the motional state information of the $S_{1/2} \rightarrow D_{5/2}$ transition. The electron-shelving method is applied to detect the electronic state of the ion.

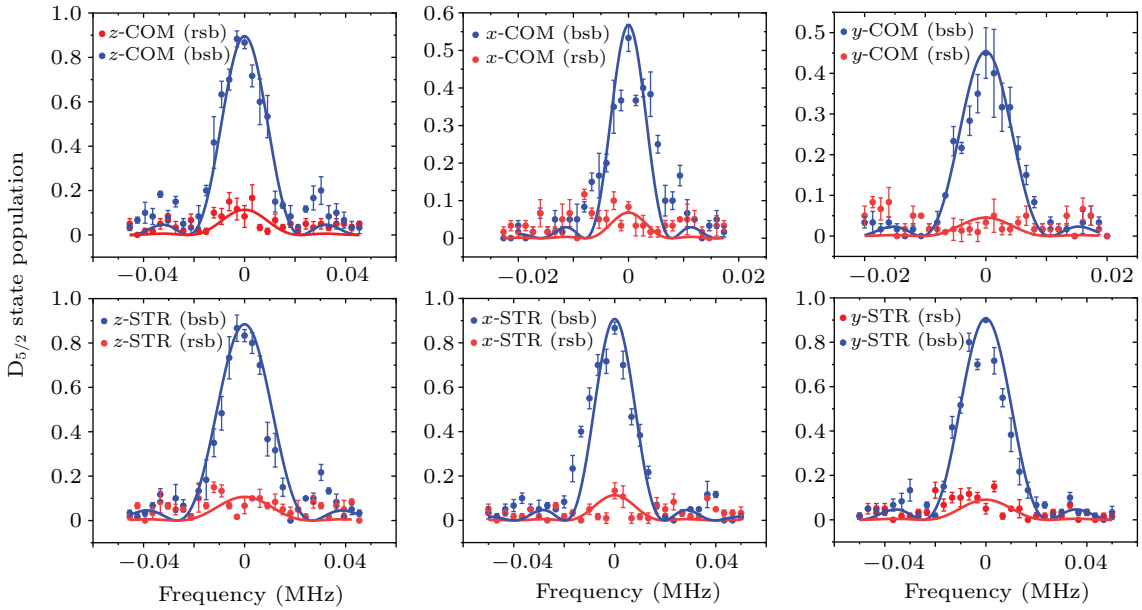


Fig. 3. The radial and axial mode spectrums of $^{40}Ca^+$–$^{27}Al^+$ ion crystal after 2 ms of Doppler cooling and a subsequent 1 ms EIT cooling. The σ^+ polarized light induced ac Stark shift is set to $2\pi \times 2.5$ MHz. The obvious drop in the red sideband indicates that EIT cooling is achieved simultaneously with all radial and axial modes spread over a range of 3 MHz of cooling.

In our experiments, we investigated the EIT cooling of a pair of $^{40}Ca^+$–$^{27}Al^+$ ion crystals in a linear Paul trap. To achieve all the radial and axial modes cooled simultaneously, the ac Stark shift induced by the σ^+ polarized light was set in the middle of the motional mode frequencies at approximately 2.5 MHz roughly. As shown in Fig. 3, all the red sidebands disappeared after applying a 1 ms EIT cooling pulse, indicating that all modes of the $^{40}Ca^+$–$^{27}Al^+$ ion crystal are simultaneously cooled to the ground state of motion. The mean phonon number can be measured with laser excitation in the narrow quadrupole transition of $S_{1/2} \rightarrow D_{5/2}$ at 729 nm using, where P_r (P_b) donates the first red (blue) sideband excitation probability of the $S_{1/2} \rightarrow D_{5/2}$ transition. In our experiments, the average number of phonons for each mode is $\bar{n}_{x\mathrm{com}} = 0.15 \pm 0.02$, $\bar{n}_{y\mathrm{com}} = 0.15 \pm 0.02$, $\bar{n}_{x\mathrm{str}} = 0.12 \pm 0.03$, $\bar{n}_{y\mathrm{str}} = 0.13 \pm 0.02$, $\bar{n}_{z\mathrm{str}} = 0.09 \pm 0.01$, and $\bar{n}_{z\mathrm{com}} = 0.15 \pm 0.02$, respectively. We also evaluated the initial temperature of each mode after Doppler cooling.

The results are $\bar{n}_{x\mathrm{com}} = 6.98 \pm 0.82$, $\bar{n}_{y\mathrm{com}} = 5.65 \pm 0.49$, $\bar{n}_{x\mathrm{str}} = 5.23 \pm 0.42$, $\bar{n}_{y\mathrm{str}} = 3.02 \pm 0.26$, $\bar{n}_{z\mathrm{str}} = 12.84 \pm 0.86$, and $\bar{n}_{z\mathrm{com}} = 7.51 \pm 0.86$, respectively. The errors are calculated based on the error of the least-square fit. Impure circularly polarized light may limit the cooling results. In the future, Ramsey experiments[22] could be used to optimize polarization more precisely.

As shown in Fig. 4, we take the z-COM mode as an example to show how the mean phonon number change during the EIT cooling pulse. After the $^{40}Ca^{+}$–$^{27}Al^{+}$ ion pair was applied to Doppler cooling for 2 ms, the varied pulse time of the EIT cooling was applied. After the cooling step, a ratio of red sideband to blue sideband is performed to determine the mean phonon number. An exponential function was used to fit the data:[22] where A is a constant and representing an offset term. The fitting yields a cooling time constant of 390 μs. The mean phonon number decreases exponentially with increasing EIT cooling pulse length and well below $\langle n \rangle = 1$ after just 50 μs. The cooling rate fitted according to the experimental data in Fig. 4 is 9320 phonon/s. We theoretically calculate that the cooling rate is 9465 phonon/s and the parameters of this calculation are $\eta = 0.192$, $\Omega_\sigma = 0.84\Gamma$, $\Omega_\pi = 0.04\Gamma$, $\Delta = 3.5\Gamma$. Here Γ is linewidth of the $S_{1/2} \rightarrow P_{1/2}$ transition. The experimental and theoretical cooling rates coincide in orders of magnitude. In addition, the possible reason why the measurements does not reach the theoretical calculation limit is that the Zeeman sublevels of $^{40}Ca^{+}$ are an imperfect realization of the ideal Λ level scheme. Off-resonant coupling to $\left|P_{1/2}, m = 1/2\right\rangle$ level increases the minimum achievable mean phonon number.

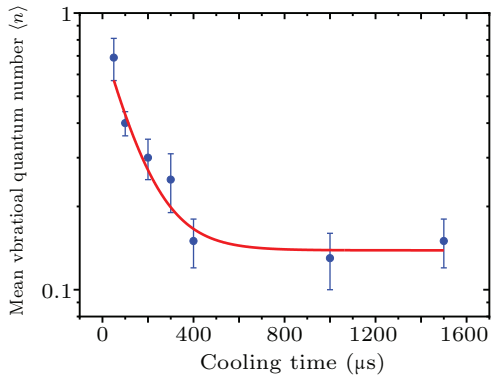


Fig. 4. Mean vibrational quantum number of z-COM mode vs. EIT cooling time. An exponential function is used to fit this cooling process.

Table 1. Measured heating rate for various modes of $^{40}Ca^{+}$–$^{27}Al^{+}$ ion crystal.

Mode	Heating rate (quanta/s)
x-COM	25.0±0.2
x-STR	7.4±0.2
y-COM	27.6±0.3
y-STR	9.5±0.1
z-COM	90±0.5
z-STR	10±0.3

We measured the heating rate of various modes of $^{40}Ca^{+}$–$^{27}Al^{+}$ ion crystal experimentally. After the EIT cooling is performed, we add a waiting period for the ions to be heated by the external environment. Then, the light at 729 nm was employed for motional state detection. Finally, the mean phonon number is calculated using the ratio of the red sideband and blue sideband of the $S_{1/2} \rightarrow D_{5/2}$ transition. The heating rate of all modes of $^{40}Ca^{+}$–$^{27}Al^{+}$ ion crystal is shown in Table 1. This result is lower than the heating rate of our previous ion trap.[26]

After EIT cooling, there is no additional cooling light during clock interrogation, and the light shift is eliminated in previous $^{27}Al^{+}$ optical clock.[31] The average phonon number during a clock interrogation can be expressed as[10]

$$\langle n(t) \rangle = \bar{n}_0 + \frac{1}{2}\dot{\bar{n}}t, \tag{4}$$

where $\bar{n}_0$ is the average phonon number after ground cooling and $\dot{\bar{n}}$ is the heating rate. For a 10 ms clock interrogation, the secular motion shift is 9.5×10^{-19}. In Doppler cooling scheme,[31] the secular motion shift and light shift are 8×10^{-18}. Therefore, the EIT cooling scheme reduces the frequency shift by an order magnitude compared to the previous Doppler scheme.

4. Conclusion and perspectives

In conclusion, the multi-mode sympathetic EIT cooling techniques for a $^{40}Ca^{+}$–$^{27}Al^{+}$ ion pair are investigated. We achieve the ground state cooling of the radial modes and axial modes of the $^{40}Ca^{+}$–$^{27}Al^{+}$ ion pair using this method efficiently. Our experiments demonstrate that EIT cooling enables sufficient cooling over a wide frequency spectrum. The cooling times are measured well below 1 ms. The heating rate of all modes of the $^{40}Ca^{+}$–$^{27}Al^{+}$ ion pair is also measured. This work is useful for quantum computing and quantum simulations based on sympathetically cooled trapped ions. It also opens a way of reducing the time dilation shift due to the secular motion in optical clocks based on $^{27}Al^{+}$ ions. A similar scheme can be applied to control the secular motion shift of multiple $^{40}Ca^{+}$ ions and $^{171}Yb^{+}$ ions in the future.

Acknowledgements

We thank Dr. Li Ji and Professor C. F. Roos for useful discussions.

Project supported by the National Key R&D Program of China (Grant No. 2017YFA0304401), the Technical Innovation Program of Hubei Province (Grant No. 2018AAA045), and the National Natural Science Foundation of China (Grant No. 11904387).

References

[1] Leibfried D, Blatt R, Monroe C and Wineland D 2003 *Rev. Mod. Phys.* **75** 281

[2] Urvoy A, Vendeiro Z, Ramette J, Adiyatullin A and Vuletić V 2019 *Phys. Rev. Lett.* **122** 203202

[3] Kippenberg T J and Vahala K J 2008 *Science* **321** 1172

[4] Porras D and Cirac J I 2004 *Phys. Rev. Lett.* **92** 207901

[5] Blatt R and Roos C F 2012 *Nat. Phys.* **8** 277

[6] Berkeland D J, Miller J D, Bergquist J C, Itano W M and Wineland D J 1998 *J. Appl. Phys.* **83** 5025

[7] Schmidt P O, Rosenband T, Langer C, Itano W M, Bergquist J C and Wineland D J 2005 *Science* **309** 749

[8] Monroe C and Kim J 2013 *Science* **339** 1164

[9] Feng L, Tan W L, De A, Menon A, Chu A, Pagano and Monroe C 2020 *Phys. Rev. Lett.* **125** 053001

[10] Chen J S, Brewer S M, Chou C W, Wineland D J, Leibrandt D Rand Hume D B 2017 *Phys. Rev. Lett.* **118** 053002

[11] Barwood G B, Huang G, Klein H A, Johnson L A M, King S A, Margolis H S, Szymaniec K and Gill P 2014 *Phys. Rev. A* **89** 050501

[12] Huntemann N, Sanner C, Lipphardt B, Tamm C and Peik E 2016 *Phys. Rev. Lett.* **116** 063001

[13] Cao J, Yuan J, Wang S, Zhang P, Yuan Y, Liu D, Cui K, Chao S, Shu H, Lin Y, Cao S, Wang Y, Fang Z, Fang F, Li T and Huang X 2022 *Appl. Phys. Lett.* **120** 054003

[14] Diedrich F, Bergquist J C, Itano W M and Wineland D J 1989 *Phys. Rev. Lett.* **62** 403

[15] Monroe C, Meekhof D M, King B E, Jefferts S R, Itano W M, Wineland D J and Gould P 1995 *Phys. Rev. Lett.* **75** 4011

[16] Lin Y, Gaebler J P, Tan T R, Bowler R, Jost J D, Leibfried D and Wineland D J 2013 *Phys. Rev. Lett.* **110** 153002

[17] Rosenband T, Hume D B, Schmidt P O, Chou C W, Brusch A, Lorini L, Oskay W H, Drullinger R E, Fortier T M, Stalnaker J E, Diddams S A, Swann W C, Newbury N R, Itano W M, Wineland D J and Bergquist J C 2008 *Science* **319** 1808

[18] Brownnutt M, Kumph M, Rabl P and Blatt R 2015 *Rev. Mod. Phys.* **87** 1419

[19] Morigi G, Eschner J and Keitel C H 2000 *Phys. Rev. Lett.* **85** 4458

[20] Morigi G 2003 *Phys. Rev. A* **67** 033402

[21] Roos C F, Leibfried D, Mundt A, Schmidt-Kaler F, Eschner J and Blatt R 2000 *Phys. Rev. Lett.* **85** 5547

[22] Lechner R, Maier C, Hempel C, Jurcevic P, Lanyon B P, Monz T, Brownnutt M, Blatt R and Roos C F 2016 *Phys. Rev. A* **93** 053401

[23] Xia K and Evers J 2009 *Phys. Rev. Lett.* **103** 227203

[24] Brewer S M, Chen J S, Hankin A M, Clements E R, Chou C W, Wineland D J, Hume D B and Leibrandt D R 2019 *Phys. Rev. Lett.* **123** 033201

[25] Ma Z, Liu H, Wei W, Yuan W, Hao P, Deng Z, Che H, Xu Z, Cheng F, Wang Z, *et al.* 2020 *Appl. Phys. B* **126** 1

[26] Cui K F, Shang J J, Chao S J, Wang S M, Yuan J B, Zhang P, Cao J, Shu H L and Huang X R 2018 *J. Phys. B: At. Mol. Opt. Phys.* **51** 045502

[27] Shang J J, Cui K F, Cao J, Wang S M, Chao S J, Shu H L and Huang X R 2016 *Chin. Phys. Lett.* **33** 103701

[28] Wubbena J B, Amairi S, Mandel O and Schmidt P O 2012 *Phys. Rev. A* **85** 043412

[29] Chao S J, Cui K F, Wang S M, Cao J, Shu H L and Huang X R 2019 *Chin. Phys. Lett.* **36** 120601

[30] Guggemos M, Heinrich D, Herrera-Sancho O A, Blatt R and Roos C F 2015 *New J. Phys.* **17** 103001

[31] Cui K, Chao S, Sun C, *et al.* 2022 *Eur. Phys. J. D* **76** 140

[32] Hettrich M, Ruster T, Kaufmann H, Roos C F, Schmiegelow T, Schmidt-Kaler F and Poschinger U G 2015 *Phys. Rev. Lett.* **115** 143003

[33] Sauter T, Neuhauser W, Blatt R and Toschek P E 1986 *Phys. Rev. Lett.* **57** 1696

[34] Bergquist J C, Hulet R G, Itano W M and Wineland D J 1986 *Phys. Rev. Lett.* **57** 1699

[35] Kielpinski D, King B E, Myatt C J, *et al.* 2000 *Phys. Rev. A* **61** 032310

[36] Lounis B and Cihen-Tannoudji C 1992 *J. Phys.* II *France* **2** 579

[37] Eschner J, Morigi G, Schmidt-Kaler F and Blatt R 2003 *J. Opt. Soc. Am. B* **20** 1003